Review Article

# Metabolic Imaging and Other Applications of Hyperpolarized $^{13}C$[1]

Klaes Golman, PhD, J. Stefan Petersson, PhD

**Key Words.** MRI; hyperpolarized $^{13}C$; metabolism; flow; perfusion.

Magnetic resonance imaging (MRI) is the only imaging modality that can deliver information about the molecular structure of an injected compound. Unfortunately, MRI has a relatively low sensitivity compared to other imaging modalities (ultrasound, SPECT, PET), and there is a need to improve the fundamental imaging parameters signal-to-noise ratio (SNR) and the contrast-to-noise ratio (CNR). Proton MRI reveals soft tissue morphology in detail, and contrast media containing either Gd-chelates or Fe-oxides have been developed to increase the CNR and, in addition, improve the diagnostic yield by providing functional information in the form of flow and perfusion measurements.

In order to obtain chemical structure information one has to use magnetic resonance spectroscopy (MRS) and its usefulness as a tool in in vivo biological diagnosis has been established. In vivo MRS of nuclei other than $^{1}H$ (e.g., $^{31}P$ and $^{13}C$) has extended our knowledge of metabolism (1) and the study of intermediary metabolism of biomolecules has given valuable insight into the fundamental of disease processes (2). The MRS technique used in those studies does not, however, allow acquiring images in a medically relevant time frame of seconds.

In a MRI scanner operating at 1 T or higher, where the dominating sources of noise is the patient, the SNR may be expressed according to

$$SNR \propto \gamma\, P\, c = \gamma^2\, B_o\, c \qquad (1)$$

Where $\gamma$ is the gyromagnetic ratio of the nuclei in question, $P$ is the polarization and $c$ is the concentration of the signal generating nuclei. In the right hand side of the expression, the polarization has been divided into a $\gamma$-factor, and the main magnetic field ($B_o$). At a magnetic field of 1.5 T, the polarization of the protons ($^{1}H$) at body temperature is only $\approx 5 \times 10^{-6}$ and for $^{13}C$ $\approx 1.0 \times 10^{-6}$.

The expression indicate that if the level of polarization is created by an external "polarizer system," that is, outside of the scanner, the obtained SNR values will no longer be a function of the main magnetic field of the used imaging system. The term *hyperpolarization* has been introduced to describe the situation when a nonthermal equilibrium level of polarization has been created. The population difference between the two possible energy states for a spin ½ nuclei may be altered by several orders of magnitude. Consequently, visualization of nuclei of low concentration may, due to the process of hyperpolarization, result in images with a high SNR.

In the mid 1990s, the first in vivo imaging experiment, taking advantage of a hyperpolarization methods, were reported (3, 4). The noble gases $^{3}He$ and $^{129}Xe$ were hyperpolarized in devices based on optical pumping using a laser source. After inhalation of a hyperpolarized gas, it was possible to generate images showing the air space of the lungs. Several groups extended the initial spatial imaging approach into applications where it has been possible to obtain regional $pO_2$ measurements in the lungs (5) and regional ventilation maps (6) as well as alveolar size information (7). Although various carriers have been proposed as delivery medias for gases (8, 9), the in vivo results using hyperpolarized gases as intravascular imaging agents have been very disappointing, and resulting in images with low SNR.

The resent developments of hyperpolarization methods for $^{13}C$ (10–14) have opened a new field of in vivo application. An injectable hyperpolarized solution may be used to

**Acad Radiol 2006;** 13:932–942

[1] From Amersham Health R&D AB, part of GE Healthcare, Medeon, SE-20512 Malmö, Sweden (K.G.), and GE Healthcare, Berga Allé 1, SE-254 52 Helsingborg, Sweden (J.S.P.). Received xxx, 2006; accepted xxx, 2006. **Address correspondence to:** J.S.P. e-mail: Stefan.Petersson@ge.com


doi:10.1016/j.acra.2006.06.001

visualize part of the vascular system, to map physiological parameters (e.g., perfusion) or probe metabolic pathways.

The purpose of this paper is to review the suggested applications of hyperpolarized solutions based on molecules containing hyperpolarized $^{13}C$. The instrument/scanner modifications needed in order to take advantage of the gained polarization will be discussed together with the limitations implied by using $^{13}C$ as the imaged nucleus.

## HYPERPOLARIZATION TECHNIQUES

Two different hyperpolarization approaches have been presented for in vivo work using $^{13}C$-containing organic molecules: para-hydrogen-induced hyperpolarization (PHIP) (10–12) and dynamic nuclear polarization (DNP) (13, 14). The PHIP method and the DNP methods have been reported to produce 20%–40% polarization in a number of different $^{13}C$-labeled substances. The DNP method (13) is a general method and may be applied to all nuclei ($^{1}H$, $^{13}C$, $^{15}N$, etc.) in virtually all molecules, while the PHIP method only can be used for polarization of $^{13}C$ in a limited number of molecules. Basically, the PHIP method takes advantage of simpler equipment than the DNP method and can produce more than 20% polarization in a few seconds, while the DNP method requires 30–60 minutes to reach the same degree of polarization.

## HYPERPOLARIZED $^{13}C$ IMAGING AGENTS

The pharmacokinetic and pharmacological behavior of the imaging agent will depend on the chosen molecule only, since the hyperpolarization as such does not change any chemical or physical properties of the substance. The first in vivo $^{13}C$ imaging experiments used nonendogenous and biological nonactive substances to produce angiographic images. Results using the PHIP methods with hydroxyethylpropionate (10, 15) and using the DNP method with 1,1-bis(hydroxymethyl)-cyclopropane-(1-$^{13}C$,D8) (16) have shown that $^{13}C$ imaging is feasible. Imaging, using hyperpolarized $^{13}C$-labeled urea, indicates that it is possible to use endogenous substances to obtain similar results (17). Recently, in vivo imaging has been performed using a hyperpolarized metabolic active substance, and real time imaging of metabolism has been demonstrated with 1-$^{13}C$–labeled pyruvate as a metabolic marker (18).

In order to have $T_1$ long enough, to make a $^{13}C$-containing molecule clinical useful, its molecular weight should be in the range of only a few hundred atomic mass units (u). The $T_1$ of currently available $^{13}C$ substances are short, compared to the half-life of nuclei used in clinical PET procedures (e.g., $^{18}$fluoro-deoxyglucose [FDG]). Consequently, no advance chemical synthesis may be performed after the polarization procedure. However, the general DNP polarization process may be applied to a wide range of small organic molecules to obtain an injectable water solution with clinical acceptable relaxation times. Reported $T_1$ and $T_2$ values of the $^{13}C$-containing molecules, used in in vivo imaging experiments, are typically 10–100 times longer than those of $^{1}H$ resulting in in vivo values of $T_1$ ≈20–45 seconds and $T_2$ ≈2–5 seconds (17, 19, 20).

## ADOPTION OF AN MRI SCANNER FOR HYPERPOLARIZED IMAGING

In order to perform imaging experiments, using a hyperpolarized $^{13}C$ substance, the MRI scanner system need to be able to send and receive on the carbon resonance frequency of molecule in question. The frequency will be linear function of the main magnetic field. At 1.5 T, the proton resonance frequency is ≈60 MHz but the $^{13}C$ resonance frequency is, due to the low $\gamma$-value, only ≈15 MHz. All the major manufacturers of MRI scanners sell "multinuclei" hardware/software to their high-end system users. This extension will, in most cases, enable the scanner to operate in a frequency window suitable for hyperpolarized $^{13}C$ imaging. Dedicated RF coils, tuned to the $^{13}C$ frequency, are needed. Since the built-in whole body transmit coil in the scanner system is tuned to the proton frequency, the $^{13}C$ coils need to be of send-and-transmit type. In order to be able to perform scout and positioning using proton imaging protocols, the scanner system should allow for switching between the proton frequency and the $^{13}C$ frequency while the object/patient remains at a fixed position in the scanner. All images shown in the present works were generated using a custom-made two-element quadrature $^{13}C$ transmit/receive coil (Rapid Biomedical GmbH, Würzburg, Germany) with a inner diameter and length of 260 mm and 350 mm, respectively.

The low gyromagnetic ratio will also have an impact on the spatial encoding procedure. The impacts from a given gradient amplitude will only be about one-fourth compared to the situation when proton imaging is performed. That is, echo times (TE) and repetition time (TR) may be prolonged in order to obtain an image resolution comparable to the one obtained in a proton imaging protocol.

## OPTIMAL MAGNETIC FIELD STRENGTH AT HYPERPOLARIZED $^{13}C$ IMAGING

The SNR found in images generated using a hyperpolarized $^{13}C$ image agent will to a first approximation be independent of the main magnetic field of the used scanner system. This indicate that the use of hyperpolarized substances should make it possible to perform imaging at magnetic field, lower than the one used in clinical routine of today, and still generate images with high *SNR*. But in order to be able to create the images within the time frame of one $T_1$ after the injection, the highest available gradient amplitude must, in most situations, be applied. When a low magnetic field is combined with high gradient amplitudes, the nonlinear components of the gradient fields need to be considered. That is, the concomitant gradient terms (21), sometimes named the Maxwell terms, may cause image artefacts.

Assuming a cylindrical symmetry for the *z*-coil and identical *x*- and *y*-coils rotated with 90° with respect to each other, the "worst case" of geometrical distortion will appear if the slice plane is oriented along the *y*-direction, the *z*-direction is used as the phase direction, and the readout is performed along the *x*-direction. The phase evolution, due to the concomitant gradient field induced by the read gradient, during the sampling window, $\phi$ is given by

$$\phi = t_{\text{samp}}\gamma\frac{G_x^2}{2\,B_o}d^2 \qquad (2)$$

where $t_{samp}$ is the sampling time, $G_x$ is the readout gradient (along the *x*-direction), and *d* is the distance in the *z*-direction from the isocenter of the scanner. If $t_{\text{samp}} = 1$ millisecond (128 samples using a bandwidth of 150 kHz), $B_o = 0.2$ T and the applied read gradient is set to 40 mT/m, then the intra-voxular phase evolution, due to the concomitant gradient field, will introduce a pixel shift already at a distance ≈12 cm from the isocenter of the magnet. Consequently, imaging at an even lower field (<0.2 T) is only possible if lower gradient amplitudes are used, which will be translated into longer TE and TR times. This indicates that hyperpolarized $^{13}C$ imaging may not be performed in low field system if high gradient power, due to a fast imaging protocol, is needed. However, it should be noted that applications were fast imaging and/or high resolution is not needed, one may perform imaging at low field without imaging distortions due the concomitant gradient field. Low-resolution hyperpolarized $^{3}He$ images have been generated at a main magnetic field of only 3 mT (22).

Different species of $^{13}C$-containing molecules may have different resonance frequencies. The chemical shift splitting of the peaks in a given resonance spectrum will be a linear function of the main magnetic field. Consequently, in clinical metabolic $^{13}C$-imaging applications, where several $^{13}C$ substances should be visualized in separate images, a high magnetic field may be beneficial.

The results shown in the present work were all generated at a main magnetic field of 1.5 T.

## ADOPTION OF PULSE SEQUENCES AND IMAGING PROTOCOLS FOR HYPERPOLARIZED IMAGING

The MRI of the hyperpolarized $^{13}C$ substance is different from what has been applied to clinical proton imaging in a standard MRI system. A number of papers have described many of the special features (10, 19, 20, 23) that characterize the $^{13}C$ hyperpolarization imaging.

A paramagnetic contrast medium operates by altering the relaxation times of the nuclei in the surrounding tissues. That is, the signal is generated not by the injected substance, but by the hydrogen nuclei in mainly the water molecules. A hyperpolarized imaging agent will, during an imaging experiment, be the source of the detected NMR signal. The concentration of protons in blood is ≈80 M. The $^{13}C$ concentration in the injected hyperpolarized solution will be in the order of 0.3–0.5 M, and because the transport time from the intravenous injection site the to the area of interest in the human body is 2–4 seconds to reach the lung, 4–6 seconds to reach the heart, and 15–30 seconds to reach most of the major organs, the magnetization will decay due to relaxation. This, in combination with the dilution due to cardiac output and after passage of the lungs, may result in an active concentration of $^{13}C$ in the order of ≈10 mM or less in the blood. But even one $T_1$ after the injection, the available signal in the vascular system will be at least a factor of 2 higher than the one found in proton imaging at 3 T (17). An important aspect of a hyperpolarized imaging agent is the total lack of background signal. The signal from the thermal equilibrium polarized $^{13}C$ nuclei, present in the object, is far below the detection limit. Consequently, the detected MR signal, following an administration of hyperpolarized $^{13}C$, emanates from the injected substance only. This is different compared to conventional proton imaging, where injected contrast media affects the protons relaxation times in the vicinity of the paramagnetic molecules. During hyperpolarized $^{13}C$ imaging, there is no background signal other than


**Figure 1.** Intra-arterial injection of a hyperpolarized $^{13}C$ substance. The vessels in the head of the pig are depicted. The TR and TE of the used balanced SSFP pulse sequence were 4.6 milliseconds and 2.3 milliseconds, respectively.

noise from the patient and the coil/receiver system. This makes a number of imaging procedures simpler (i.e., there will not be a need for construction of subtraction images).

The $T_1$ value of a given substance will dictate what signal amplitude one may expect in the imaging area at a given time after the injection. The long $T_2$ values are beneficial for most imaging pulse techniques and may be explored in multiecho imaging strategies. However, the applied pulse sequence will always be dependent of the used imaging agent and the clinical application in question.

## CLINICAL APPLICATIONS OF HYPERPOLARIZED $^{13}C$ SUBSTANCES

The clinical applications of hyperpolarized $^{13}C$ compounds may be grouped according to

- Vascular/angiographic imaging
- Perfusion mapping
- Interventional applications
- Metabolic/molecular imaging

In the following sections, experimental imaging results from possible applications within the different categories, together with adopted pulse sequences, will be discussed. All presented results have been generated in animal studies approved by the local ethical committee in question.

### Vascular/Angiographic Imaging

In vascular and angiographic work using hyperpolarized $^{13}C$ substances, the total lack of background signal may be explored using projection imaging strategies (Fig. 1). Only vessels containing the injected substance will show up in the final images. By applying a fully balanced steady state free procession (SSFP) sequence (24), it is possible take advantage of the initial high signal amplitude, together with the long relaxations, and still reach high temporal as well as high spatial resolution. The flip angle (FA) used to generate the images in Figure 1, $\approx 90^{o}$, results in a mix of transversal magnetization components that, due to the balanced gradients, are constructive added together. Scan time for one $104 \cdot 128$ matrix image (Fig. 1) was 470 milliseconds.

To suppress flow-induced artefacts, the low $\gamma$ of carbon (only one quarter of the proton value) put demands on a high gradient slew rate and a high amplitude. The available scanner hardware, used in the image experiment, limited the TE to 2.4 milliseconds and resulted in the flow artefacts in the images (the arrow in Fig. 1c).

The dynamic filling and the extension of the coronary arteries may be visualized using an injection of a hyperpolarized $^{13}C$ substance (Fig. 2). During this experiment, performed in a pig model, a thick slice of 15 cm was used. Again, a balanced SSFP pulse sequences was used. Cardiac gating was used in combination with a SSFP sequence, with a scan time of 422 milliseconds, in order to generate an image at every heartbeat. The used sequence parameters were

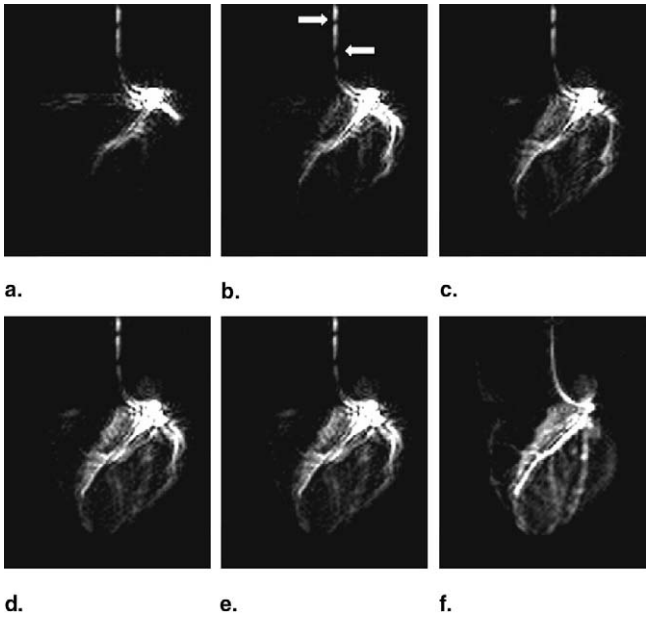


**Figure 2.** A series of hyperpolarized $^{13}C$ angiograms obtained during an injection through a catheter placed in the left coronary descending artery and left circumflex of a pig. The first diagonal branch and smaller septal branches are visualized. The artefacts, indicated with *white arrows*, are created by the fast moving spins inside the catheter. One image was acquired per heartbeat and the total scan time per image was 422 ms.

TR/TE/FA = 6.6 milliseconds/3.3 milliseconds/90°. The high velocity inside the catheter gives rise to signal cancellation artefacts indicated by the arrows in Figure 2b.

## Interventional Applications

Hyperpolarized $^{13}C$ substances may be used in several interventional applications. The extension of the vessels system may be demonstrated, the flow measured using intra-arterial injections and, when the catheter has been placed in the target organ, the perfusion may be mapped. This possible application will be discussed in more detail in the next section. However, the visualization of the catheter itself may also be done using a hyperpolarized $^{13}C$ substance (25). Figure 3 shows the results from a catheter tracking experiment. A commercial three-lumen catheter was modified in order for two of the lumens to form a loop where the hyperpolarized $^{13}C$ contrast agent could flow without leaving the catheter. Projection images of the catheter have been superimposed on proton road map images. The arrows indicate the tip of the catheter. The sagittal and the coronal $^{13}C$ projection images were acquired in an interleaved fashion and the total scan time per projection was 300 milliseconds. The three-dimensional proton road map was collected before the $^{13}C$ projection imaging and the image fusion was performed offline. In a future implementation of the catheter tracking procedures, one may envision an interleaved collection of the proton and the $^{13}C$ image data combined with a real-time fusion software package. This would allow for an interactive clinical procedure where the clinician would be able to see the catheter, with reasonable high frame rate, superimposed on proton images with high soft-tissue contrast.

The interventional procedure may be extended to show not only the catheter but also the injected substance. This application is illustrated in the time series shown in Figure 4. The possibility for direct imaging of the injected substance may be used to show viability during therapeutic procedures. In the first image (Fig. 4a), the $^{13}C$ projection image of the catheter has been superimposed, and color coded (green), on the proton roadmap. The tip of the catheter was placed in the right renal artery. In the following images (Fig. 4b–f), the $^{13}C$ projection images, obtained during the injection through the catheter of the hyper polarized substances, have been color coded (hot iron scale) and superimposed on the same proton road map. This way of combining and visualization of the injected $^{13}C$, together with the catheter visualization, may be extended to procedures where chemical ablation is performed.

## Perfusion Mapping

The signal obtained from the injected hyperpolarized substance is, after correction for relaxation, direct proportional to the concentration of the imaging agent in question. Consequently, a $^{13}C$ image, obtained directly after an injection, is a qualitative map of the perfusion. The images given in Figure 5a–c demonstrate the signal after an intra-arterial injection in the left coronary artery. The myocardium supplied by the left anterior descending coronary artery and the left circumflex demonstrate a homogeneous signal. After an occlusion of the left anterior descending coronary artery, no signal is measured in the part of the myocardium supplied by it (Fig. 5d–f). This way of demonstrating changes in perfusion may be used when a qualitative perfusion value, from a clinical point of view, is sufficient.

By obtaining a series of images during the passage, of bolus of a hyperpolarized $^{13}C$ substance, quantitative perfusion maps may be reconstructed (26, 27). The time series in Figure 6a–e were obtained after an arterial injection in the renal artery, similar to the one used to generate the time series in Figure 4. However, the series was generated during the outflow phase of the imaging agent. The used balanced SSFP pulse sequence applied centric phase encoding and the time delay between the images was set


**Figure 3.** $^{13}C$ catheter tracking images superimposed on proton roadmaps. The tip of the catheter is indicated by the *arrows*. The $^{13}C$ projection images were generated when the hyperpolarized $^{13}C$ substance only circulated through a double-lumen catheter. The scan time per projection was 300 milliseconds.

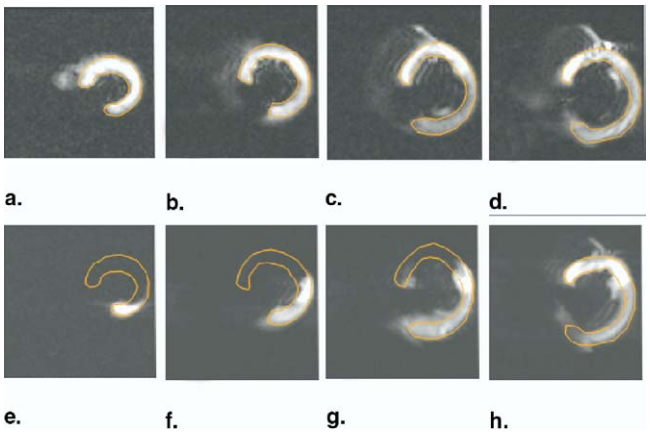


**Figure 4.** A series of interventional $^{13}C$ images superimposed on a proton road map. In the first images (*a*), only the green color-coded catheter is shown. This image was generated during the circulation of a hyperpolarized $^{13}C$ substance through the catheter. The rest of the series (*b-f*) were obtained during the intra arterial injection of a hyperpolarized $^{13}C$ substance in the right renal artery.

to 2 seconds. This time series allows for correction of the relaxation effects and signal decay due to excitation pulses during the imaging generation and allows for the generation of "a relaxation and decay map" (Fig. 6f). The final quantitative perfusion map is shown in Figure 6g, superimposed on the corresponding proton image. It should be noted that in order to be able to perform this calculation, information regarding the extraction and the partition coefficient needs to be known.

Perfusion mapping is not restricted to arterial injections through a catheter; instead it may be performed after an intravenous injection of the hyperpolarized $^{13}C$ substance. The possibility of use this approach have been evaluated in a pig heart model (Figure 7). Due to the short distance between the ejection point and the heart, the polarization of the bolus is still high when it reaches the image volume. The imaging loop was initialized before the hyperpolarized bolus reached the heart and a time series was obtained (Fig. 7a–I). By applying the Kety-Schmidt method (28), it was possible, on a pixel-to-pixel bases, to calculate a quantitative myocardium perfusion map. The obtained quantitative perfusion map may then be superimposed on the corresponding proton slice (Fig. 7j). During this experiment, the data collection was cardiac triggered, and one image was generated every second heartbeat. A balanced SSFP pulse sequence was used, and the following parameters were applied: TR/TE/FA =

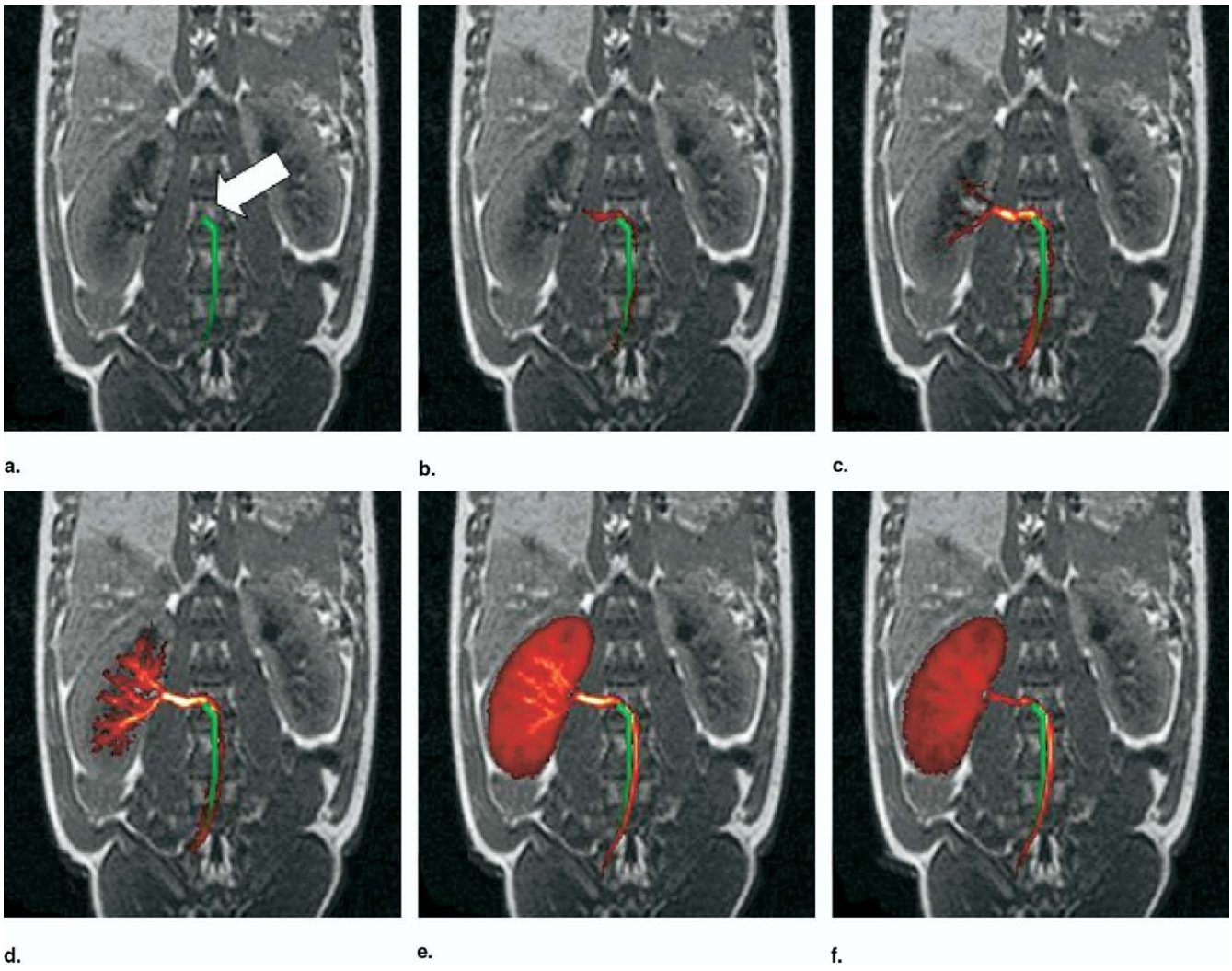


**Figure 5.** Qualitative perfusion mapping during a coronary artery occlusion experiment. The images in the top row (*a–d*) show the four slices obtained after an intra-arterial injection of hyperpolarized $^{13}C$ in the left anterior descending coronary artery and the left circumflex artery in a pig heart. The images in the bottom row (*e–h*) show the same slices after an occlusion of the left anterior descending coronary artery and a second injection of $^{13}C$. The outline of the signal-generating part of the myocardium before the occlusion has been superimposed on the images. The first three images (*e–g*), obtained after the occlusion, corresponding to the basal part of the heart, demonstrate a signal void in the affect area. In the last image (*h*), corresponding to a slice positioned above the affected area, no signal reduction is seen.

6.7 milliseconds/3.3 milliseconds/30°, pixel size 3 × 3 × 10 $mm^3$, matrix size 64 × 64, and the scan time per image was 470 milliseconds.

## METABOLIC/MOLECULAR IMAGING

Since hyperpolarized $^{13}C$ MRI directly informs about the molecule, to which the hyperpolarized atoms are attached, investigation of tissue and cell viability (direct molecular imaging) is feasible. While SPECT and PET only visualize the distribution of the active nuclei, regardless if they are still contained within the injected molecule or not, NMR is capable of distinguishing signals from the tracer in different molecules (17, 19). The visualization of the different $^{13}C$-containing molecules will depend on the spectral peak separation and is performed by applying a chemical shift imaging (CSI) pulse sequence. The method makes it possible to generate frequency information simultaneously with spatial information.

By injection of hyperpolarized $^{13}C_1$-pyruvate, it is possible to study the major generating metabolic and catabolic pathways in mammalian cells. Pyruvate is a substrate at a

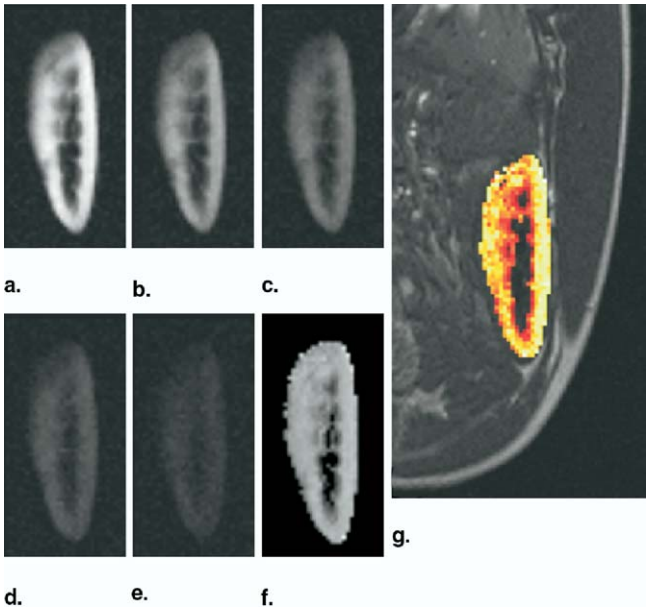


**Figure 6.** Quantitative renal perfusion mapping. The outflow series (*a–e*), measured after an intra-arterial renal injection, have been used to calculate the decay map given in (*f*). This map is then used to calculate a quantitative perfusion map. The color-coded perfusion map is in (*g*) superimposed on the corresponding proton slice.

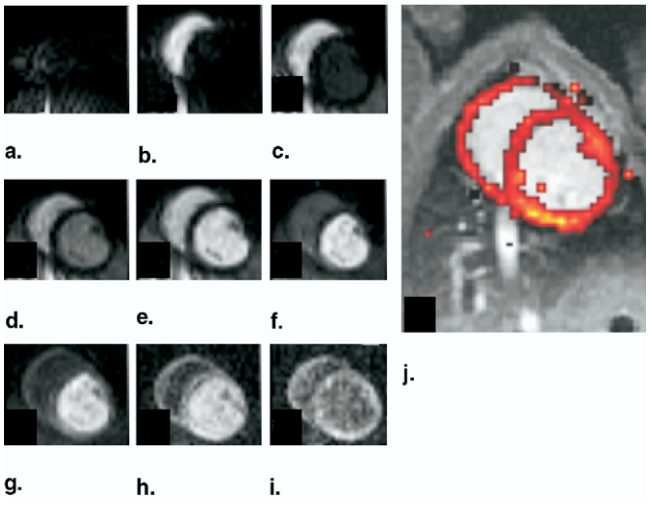


**Figure 7.** Quantitative myocardium perfusion mapping. A time series (*a–i*) obtained during the bolus passage through the heart after an intravenous injection of a hyperpolarized $^{13}C$ substance. Using the Kety-Schmidt model, the perfusion was be calculated on a pixel-to-pixel bases. The color-coded perfusion map has been superimposed on the corresponding proton slice in (*j*).

central cross-road of metabolic reactions (29, 30), leading to energy production as well as the formation of lactate, alanine, and carbon dioxide (Figure 8). The carbon dioxide ($CO_2$) is in rapid equilibrium with bicarbonate ($HCO_3^-$).

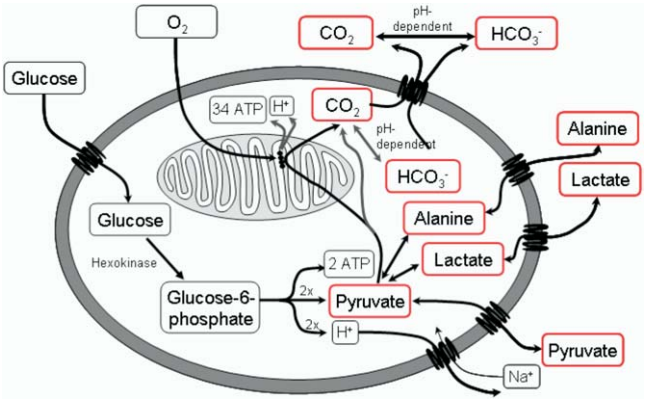


**Figure 8.** The metabolic pathways in the cells of endogenous glucose and endogenous/injected pyruvate. The metabolic products that can be imaged using the hyperpolarized $^{13}C$-pyruvate technique are shown in red.

Since the resonance frequencies of the metabolic products produced from pyruvate will be sufficiently separated from the frequency of pyruvate itself, it will be possible to follow the $^{13}C$ atom through the metabolic steps. The relative amount of the produced metabolites will be a function of the actual condition of the cells, including viability parameters such as $Po_2$ and pH. The ratio between $CO_2$ and $HCO_3^-$ in tissue is directly related to the pH and a low concentration of $HCO_3^-$ may therefore be explained by a low pH in the examined area.

It is known that pyruvate in cancer cells is transformed to lactate through anaerobic glycolysis (31). This change in metabolic pattern, compared to normal cells, may be used to detect and presumably also to visualize the extension of a tumor. By applying metabolic imaging it is possible to create images mapping the concentration and ratio between lactate and alanine formed and pyruvate present in the cells, thereby enabling an indirect measure of the lactate production by the cells.

Figure 9 demonstrates the metabolic pattern after an intravenous injection of hyperpolarized $^{13}C$-pyruvate in a rat with an implanted P22 tumor. The distribution of $^{13}C_1$-pyruvate and its metabolites $^{13}C_1$-alanine and $^{13}C_1$-lactate was imaged ≈35 seconds after the start of the injection of the pyruvate solution. The CSI images were generated with an in plane resolution of $5 \times 5$ mm$^2$ and slice thickness of 10 mm. The pyruvate has been partly metabolized into alanine and lactate. The distribution of lactate is given in Figure 9d, and the tumor area shows the highest concentration of lactate. Figure 9c demonstrates that the pyruvate metabolism into alanine is dominating in the muscle, and low alanine production is

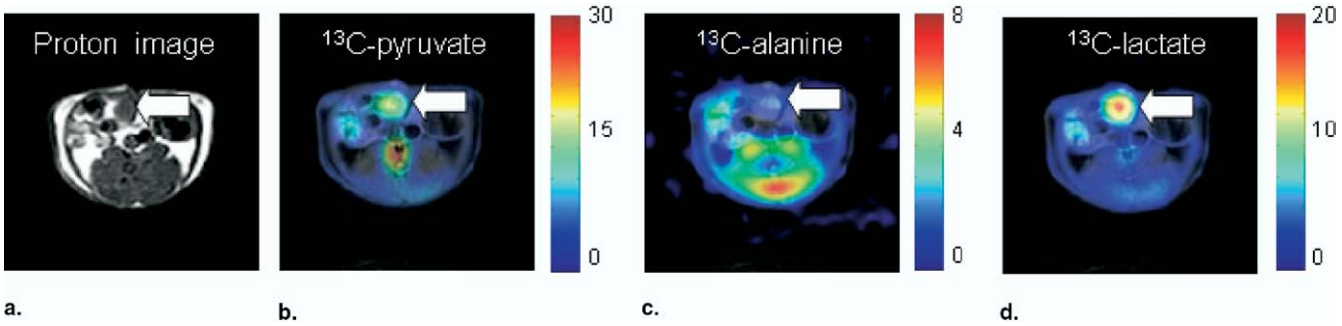


**Figure 9.** The metabolic pattern in a tumor model. Maps of the metabolites alanine (*c*) and lactate (*d*) obtained in a rat tumor model after injection of hyperpolarized $^{13}$C-pyruvate (*b*). The first image (*a*) shows the corresponding proton slice. The $^{13}$C maps have all been superimposed on the proton map. In all images, the position of the implanted tumor in indicated by a *white arrow*. All $^{13}$C images have been individually scaled.

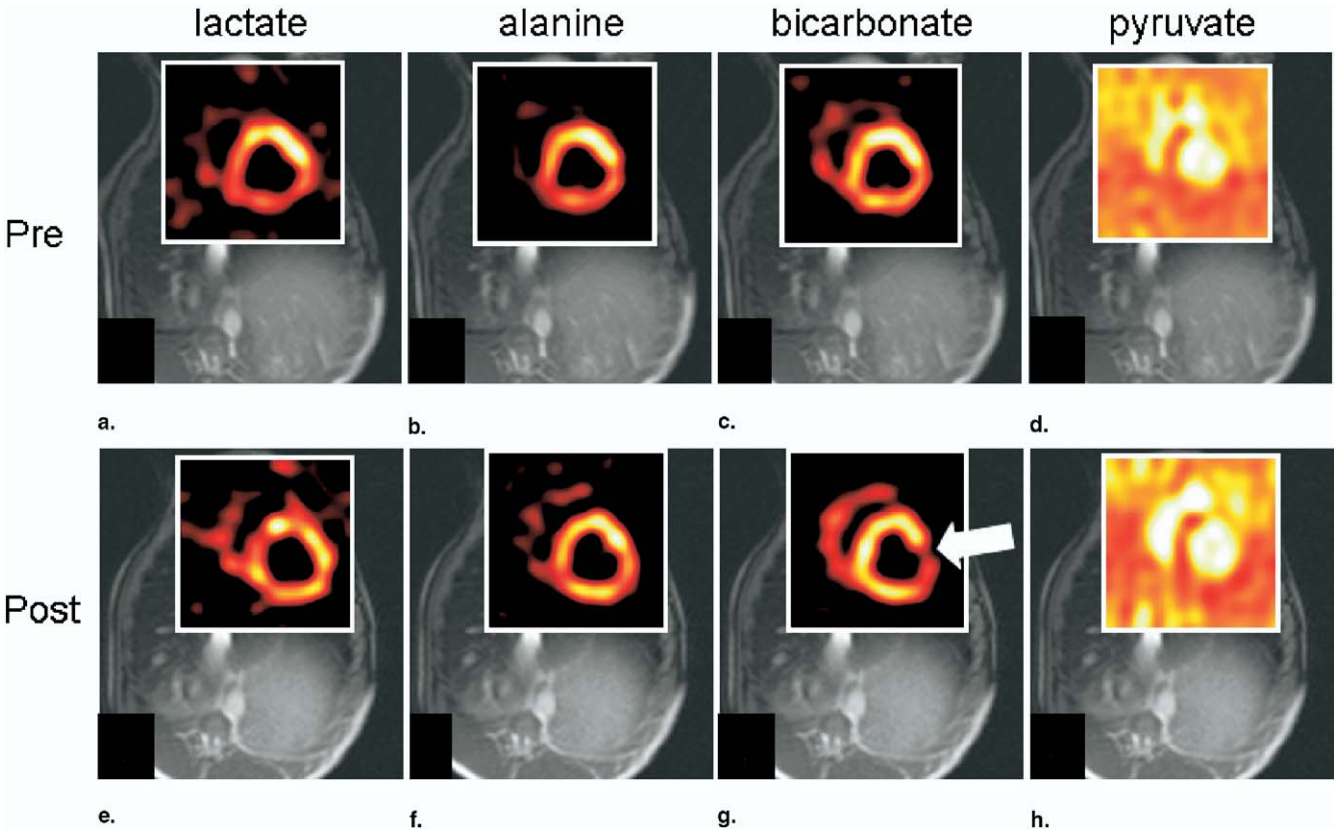


**Figure 10.** Cardiac $^{13}$C metabolic mapping during an occlusion experiment. The topmost row (*a–d*) shows metabolic pattern before the occlusion of the left circumflex. The alanine (*b*) and the bicarbonate (*c*) maps demonstrate an even distribution in the myocardium. The maps obtained after a 15-minute occlusion and a reperfusion period of 2 hours are shown in the bottom row (*e–h*). In the area affected by the occlusion, the signal reduction in the bicarbonate (*g*) is clearly demonstrated. No reduction is measured in the alanine map (*f*).

measured in this tumor type. The metabolic maps have been superimposed on the corresponding proton image.

The fate of pyruvate in the heart muscle has been described extensively both under normal conditions (32) and during different cardiac diseases (33). In the heart this is interesting as the rate of metabolism could be considered an indicator of the viability of the cells, that is, if muscle cells can return to normal after exposure to different periods of ischemia.

Hyperpolarized $^{13}C_1$-pyruvate may be used to demonstrate the changes in the metabolic pattern in the myocardium due to a localized ischemia. An animal model based

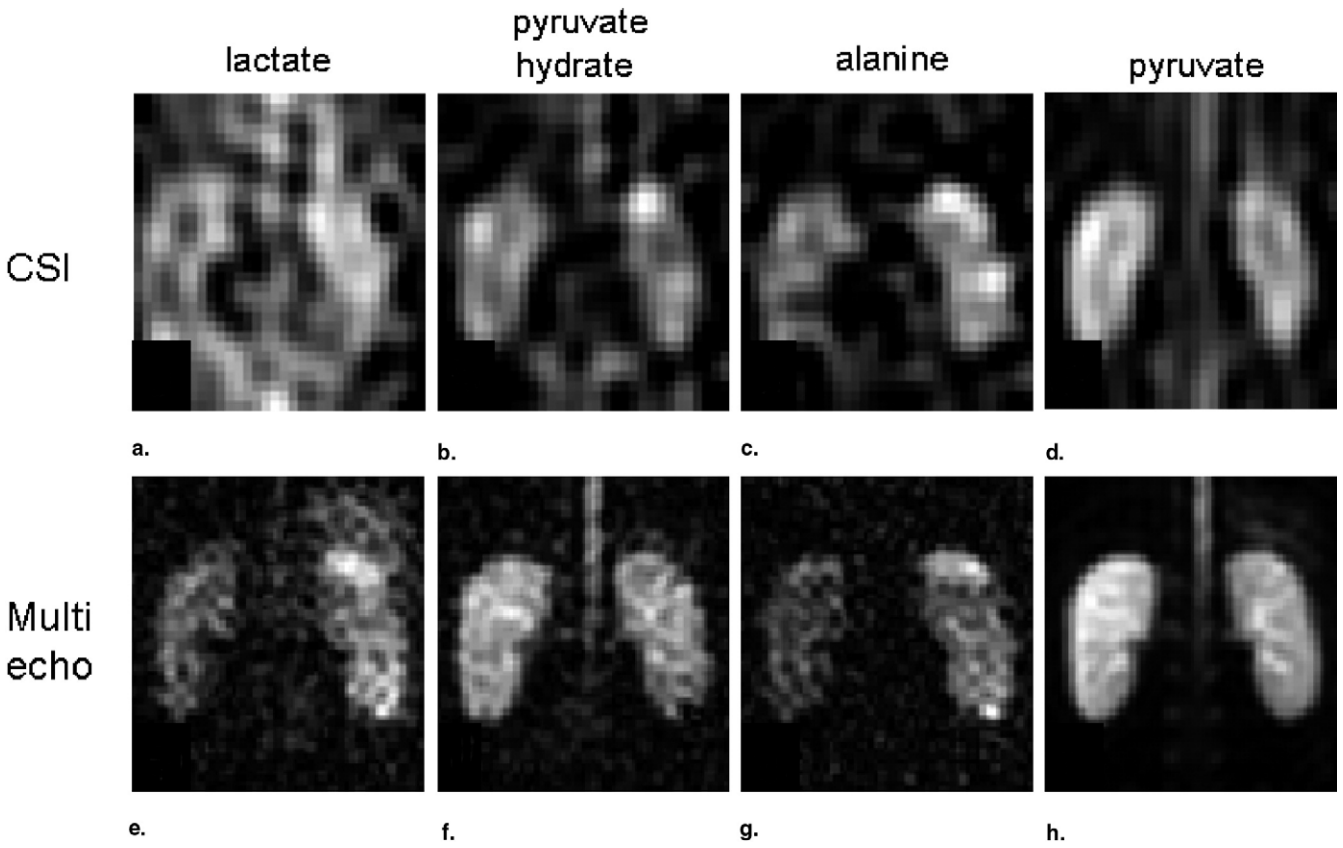


**Figure 11.** A comparison between the CSI pulse sequence (scan time = 13 seconds) and a multiecho SSFP pulse sequence (scan time = 400 milliseconds). Similar metabolic pattern and SNR are obtained with the two sequences, but the SSFP has a higher spatial and temporal resolution.

on 15-minute clamping of the left circumflex in pig heart was used to generate an ischemic area. The myocardium was reperfused for a period of 120 minutes before the imaging experiment. The obtained metabolic maps generated before and after the clamping are given in Figure 10. The pyruvate maps in this study show the distribution of $^{13}$C-pyruvate (bloodstream and myocardium). As the signal detected from a hyperpolarized nucleus is a linear function of the local concentration of the nucleus in question, the generated pyruvate maps may be regarded as qualitative perfusion maps. No reduction was seen in the pyruvate before (Fig. 10d) or after (Fig. 10h) the ischemic period. This indicates that the pyruvate reached all parts of the myocardium, including the ischemic area.

The $H^{13}CO_3^-$ generated from $^{13}$C-pyruvate shows that under normal conditions, the pyruvate dehydrogenase of the mitochondria will produce relatively large amount of $^{13}CO_2$, which turns into $H^{13}CO_3^-$ depending on the pH in the tissue. The reduced or absent bicarbonate signal (Fig. 10g) in the areas where ischemia had been present indicated that the citric acid (Krebs) cycle had been affected.

## FAST METABOLIC IMAGING

The application of hyperpolarized $^{13}$C is in its infancy and improvements are to be expected. An implementation of a multiecho SSFP pulse sequence (34, 35) was compared to the CSI pulse sequences using an animal kidney-damaging model (Fig. 11). Before the injection of 0.3 mmol/kg $^{13}C_1$-labeled hyperpolarized pyruvate, the right kidneys in a pig were exposed to 3 minutes of selective x-ray contrast medium injection and an additional 7 minutes of renal artery clamping (36). Both imaging methods were able to demonstrate the changes in metabolic pattern caused by x-ray contrast medium. The scan time of the CSI pulse sequence was ≈13 seconds but only ≈400 milliseconds when the multiecho SSFP pulse sequence was used. The resulting metabolic maps demonstrate comparable SNR; in addition, higher spatial resolution with the multiecho SSFP sequences ($7 \times 7$ mm$^2$) compared to the CSI sequence ($12.8 \times 12.8$ mm$^2$) is clearly demonstrated. This indicates that a pulse sequence adopted for the long $T_1$ and $T_2$ relaxation times, characteris-

tic for $^{13}$C-pyruvate and its metabolites, makes it possible to obtain a four-fold improvement in a 30-times shorter scan time.

## CONCLUSIONS

The use of $^{13}$C hyperpolarization is a new diagnostic platform. It may be used to perform angiographic work as well as quantitative perfusion mapping. The applications may be extended into combination approaches where the perfusion mapping approach is performed with interventional applications.

The ability to visualize the metabolic fate of pyruvate can be an important diagnostic tool to determine if the cell generates energy abnormally (cancer). In cardiac applications, it opens the possibility to show areas that, due to a period of ischemia, have an altered metabolic pattern.

The reviewed hyperpolarized $^{13}$C technique and applications should not be considered as competition to the existing proton imaging but rather as a supplement. Instead, the $^{13}$C applications may be used and combined with several already clinically established proton MRI examinations.

### REFERENCES


1. Hyder F, Brown P, Nixon TW, Behar KL. Mapping cerebral glutamate $^{13}$C turnover and oxygen consumption by in vivo NMR. Adv Exp Med Biol 2003; 530:29–39.
2. Shulman RG, Rothman DL. 13C NMR of intermediary metabolism: Implications for systemic physiology. Annu Rev Physiol 2001; 63:15–48.
3. Albert MS, Cates GD, Driehuys B, et al. Biological magnetic resonance imaging using laser-polarized $^{129}$Xe. Nature 1994; 370:199–201.
4. Middleton H, Black RD, Saam B, et al. MR imaging with hyperpolarized $^{3}$He gas. Magn Reson Med 1995; 33:271–275.
5. Deninger AJ, Eberle B, Ebert M, et al. Quantification of regional intrapulmonary oxygen partial pressure evaluation during apnea by $^{3}$He MRI. J Magn Reson 1999; 141:207–216.
6. Deniger AJ, Månsson S, Petersson JS, et al. Quantitative measurement of regional lung ventilation using $^{3}$He MRI. Magn Reson Med 2002; 48: 223–232.
7. Yablonskiy DA, Sukstanski AL, Leawoods JC, et al. Quantitative in vivo assessment of lung microstructure at the alveolar level with hyperpolarized 3He diffusion MRI. Proc Natl Acad Sci U S A 2002; 99:3111–3116.
8. Wolber J, Rowland IJ, Leach MO, Bifone A. Perfluorocarbon emulsions as intravenous delivery media for hyperpolarized xenon. Magn Reson Med 1999; 41:442–449.
9. Duhamel G, Choquet P, Leviel JL, et al. In vivo 129Xe NMR in rat brain during intra-arterial injection of hyperpolarized 129Xe dissolved in a lipid emulsion. C R Acad Sci III 2000; 323:529–536.
10. Golman K, Axelsson O, Johannesson H, et al. Parahydrogen-induced polarization in imaging: Subsecond $^{13}$C angiography. Magn Reson Med 2001; 46:1–5.
11. Jóhannesson H, Axelsson O, Karlsson M. Transfer of para-hydrogen spin order into polarization by diabatic field coupling. C R Physique 2004; 3:315–325.
12. Goldman M, Jóhannesson H, Axelsson O, Karlsson M. Hyperpolarization of $^{13}$C through order transfer from parahydrogen: A new contrast agent for MRI. Magn Reson Imaging 2005; 23:153–157.
13. Ardenkjaer-Larsen JH, Fridlund B, Gram A, et al. Increase in signal-to-noise ratio of >10,000 times in liquid-state NMR. Proc Natl Acad Sci U S A 2003; 100:10158–10163.
14. Abragam A, Goldman M. Principles of dynamic nuclear polarization. Rep Prog Phys 1978; 41:395–467.
15. Olsson LE, Chai C-M, Axelsson O, et al. Coronary angiography in pigs with intra-arterial injection of a hyperpolarized $^{13}$C substance. Magn Reson Med 2006; 55:731–737.
16. Svensson J, Månsson S, Johansson E, Petersson JS, Olsson LE. Hyperpolarized $^{13}$C MR angiography using true FISP. Magn Reson Med 2003; 50:256–262.
17. Golman K, Ardenkjaer-Larsen JH, Petersson JS, Mansson S, Leunbach I. Molecular imaging with endogenous substances. Proc Natl Acad Sci U S A 2003; 100:10435–10439.
18. Golman K, In't Zandt R, Lerche MH, Thaning M. Real-time metabolic imaging. Proc Natl Acad Sci U S A 2006; In Press.
19. Månsson S, Johansson E, Magnusson P, Chai C-M, Hansson G, Petersson JS, Ståhlberg F, Golman K. $^{13}$C imaging—A new diagnostic platform. Eur Radiol 2006; 16:57–67.
20. Golman K, Ardenkjær-Larsen JH, Petersson JS, Månsson S, Leunbach I. Molecular imaging with endogenous substances. Proc Natl Acad Sci U S A 2003; 100:10435–10439.
21. Norris DG, Hutchison JMS. Concomitant magnetic field gradients and their effects on imaging at low magnetic field strengths. Magn Reson Imaging 1990; 8:33–37.
22. Bidinost CP, Choukeife J, Tastevin G, Vignaud A, Nacher PJ. MRI of the lung using hyperpolarized $^{3}$He at very low magnetic filed (3 mT). MAGMA 2004; 16:225–258.
23. Golman K, Ardenkjær-Larsen JH, Svensson J, Axelsson O, Hansson G, Hansson L, Jóhannesson H, Leunbach I, Månsson S, Petersson JS, Pettersson G, Servin R, Wistrand LG. $^{13}$C-angiography. Acad Radiol 2002; 9:507–510.
24. Scheffler K. A pictorial description of steady-state in rapid magnetic resonance imaging. Concepts Magn Reson 1999; 11(5):291–304.
25. Axelsson O, Golman K, Månsson S, Petersson JS. International Patent Application WO2004/048988, 2004.
26. Johansson E, Månsson S, Wirestam R, Svensson J, Petersson JS, Golman K, Ståhlberg F. Cerebral perfusion assessment by bolus tracking using hyperpolarized 13C. Magn Reson Med 2004; 51(3):464–72.
27. Johansson E, Olsson LE, Månsson S, Petersson JS, Golman K, Ståhlberg F, Wirestam R. Perfusion assessment with bolus differentiation: A technique applicable to hyperpolarized tracers. Magn Reson Med 2004; 52(5):1043–51.
28. Kety SS, Schmidt CF. The nirous oxide method for quantitative determination of cerebral blood flow in man: theory, procedure and normal values. J Clin Invest 1948; 27:476–483.
29. Mallet RT. Pyruvate: Metabolic protector of cardiac performance. Proc Soc Exp Biol Med 2000 Feb; 223(2):136–148.
30. Khairallah M, Labarthe F, Bouchard B, Danialou G, Petrof BJ, Des Rosiers C. Profiling substrate fluxes in the isolated working mouse heart using 13C-labeled substrates: focusing on the origin and fate of pyruvate and citrate carbons. Am J Physiol Heart Circ Physiol 2004; 286: 1461–1470.
31. Koukourakis MI, Giatromanolaki A, Sivridis E, Gatter KC, Harris AL. Pyruvate dehydrogenase and pyruvate dehyrdrogenase kinase expression in non small cell lung cancer and tumor-associated stroma. Neoplasia 2005; 7:1–6.
32. Panchal AR, Comte B, Huang H, Dudar B, Roth B, Chandler M, Des Rosiers C, Brunengraber H, Stanley WC. Acute hibernation decreases myocardial pyruvate carboxylation and citrate release. Am J Physiol Heart Circ Physiol 2001; 281:1613–1620.
33. Lloyd SG, Wang P, Zheng H, Chatham JC. Impact of low-flow ischemia on substrate oxidation and glycolysis in the isolated perfused rat heart. Am J Physiol Heart Circ Physiol 2004; 287:H351–62.
34. Månsson S, Leupold J, Wieben O, In't Zandt R, Magnusson P, Johansson E, Petersson JS. Metabolic Imaging with Hyperpolarized $^{13}$C and Multi-Echo, Single-Shot RARE. In: Proc 14th Annual Meeting ISMRM 2006:584.
35. Leupold J, Wieben O, Månsson S, Scheffler K, Petersson JS, Hennig J. Fast Separation of Water, Acetone, Fat and Silicone with a Multiecho balanced SSFP sequence. In: Proc 14th Annual Meeting ISMRM 2006: 2444.
36. Elmståhl B. Thesis, Lund University, Sweden, 2005.